

# What Spectral Methods Can Tell Us about Heat Transfer Effects in Water Calorimeters

Ronald E. Tosh and H. Heather Chen-Mayer

National Institute of Standards and Technology, Gaithersburg, MD 20899, USA

In water calorimetry, numerous ancillary effects – such as radiation-induced chemical reactions, scattering and excess heat from nonwater materials, and dose nonuniformities within the phantom – complicate the determination of absorbed dose from measurements of radiation-induced heating. Corrections for thermal transport due to excess heat and dose nonuniformities can be difficult to assess because the effects are delayed by variable amounts of time – from seconds to hours – that depend upon the geometry of the probes, the calorimeter vessel and the radiation beam. Typically, such corrections involve finite-element modeling of these components that is analyzed in the time domain and, accordingly, is sensitive to timing details of the source. We have developed a technique that circumvents this difficulty by using periodic modulation of the radiation source and measuring an effective frequency response, or system transfer function, of the calorimeter. By tracing the frequency dependence of systematic deviations from nominal or applied dose rates due to heat conduction, our approach provides a basis for assessing systematic errors for all radiation exposure times, including those that can not be handled by data analysis techniques like midpoint extrapolation.

## Introduction

Estimates of absorbed dose from water calorimeters generally involve correction factors for effects due to heat transfer within the calorimeter. Even in the ideal case of a uniform, thermally isolated water phantom, dose gradients in the water – attributable to the beam penumbra and the depth-dose profile – would give rise to heat conduction and, in some cases, convective movement of the water that distort measurements of radiation-induced heating (proportional to absorbed dose). The temperature sensors, glass vessel, acrylic brackets and other supporting hardware used in working calorimeters aggravate this situation, introducing thermal gradients via mechanisms such as excess heat and electrical power dissipation. It is now commonplace to refrigerate the water to 4 °C [1,2], where water achieves a maximum density (hence, a zero coefficient of volume expansion), effectively shutting down convection. While this greatly simplifies the corrections needed for heat transport, particularly for horizontal radiation beams, heat conduction phenomena are unaffected.

Mathematical modeling of these effects, whether at 4 °C (without convection) or at room temperature, is complicated by the geometry of the calorimeter components: e.g. the glass vessel and probes never share the symmetry of the applied dose distribution, thus choosing an optimal coordinate system for expressing boundary conditions and source terms in the conduction-convection equations is difficult. The method of choice for determining the necessary correction factors is finite-element analysis. The typical treatment involves a geometrical model of the calorimeter components that includes relevant material parameters for purposes of estimating the thermal response to internal heating (caused by the radiation) and integration of the conduction-convection equations.

Simulations done with/without convection and/or conduction terms in the equations provide a measure of the distortions caused by heat transport and enable the determination of correction factors. Such calculations have been used to obtain simulated waveforms that are in excellent agreement with experimental data, effectively disposing of the problem of correcting for heat transport at several national metrology laboratories using water calorimeters.

However, the ability to obtain correction factors with a high degree of confidence requires good control of the initial temperature distribution throughout the phantom and the timing details of the radiation exposure – in order to duplicate conditions that can be realized in the simulations. Typically, a flat temperature distribution is established by stirring away temperature gradients within the phantom and waiting for thermal equilibrium before beginning a sequence of radiation exposures that are punctuated by pre- and post-irradiation drift periods as shown in Figure 1. The timing details within such a sequence vary from case to case – a typical instance may include up to 10 radiation shots of 60 s to 120 s duration spaced by drift periods of similar length – but must balance requirements for signal-to-noise against distortions due to heat transfer, both of which grow with exposure time. Interrupting the sequence to reestablish thermal equilibrium becomes necessary when heat-transfer distortions in the time waveform become severe enough that assumptions associated with the widely used midpoint-extrapolation technique – viz. small changes in the background temperature drift component during a single exposure period – no longer apply.

Thus, with current practice, conditions necessary for obtaining accurate correction factors for heat transfer considerably reduce the effective duty cycle for useful data acquisition. This effective duty cycle is diluted still further by the midpoint extrapolation technique itself, in which linear fits are made to the drift segments only, and large segments of the data (e.g. the irradiation zones) are neglected. A greater fraction of the data can be used if the fit is performed with a more detailed parametric model than that associated with midpoint extrapolation. If such a model incorporates effects due to heat transport, then it might even become possible to run the instrument without stirring breaks to reestablish thermal equilibrium.

The present work describes efforts in developing such a model. In contrast to the more widely accepted approaches of using midpoint extrapolation method in time domain waveforms as mentioned above, in which conditions for acceptable measurements are not permitted to stray very far from thermal equilibrium, we are exploring how internal physical processes like heat transfer affect the steady-state response of the calorimeter to periodic excitation. Operationally, this amounts to modulating the radiation heating, acquiring data over many cycles of this modulation, and then analyzing the signal waveforms in the frequency domain. By regarding the calorimeter as a sort of network whose frequency response is determined by the physics of heat conduction and convection, we evaluate the feasibility of harnessing digital filtering techniques for extracting the desired dose information from the output signal. In principle, such an approach should enable measurements to be conducted continuously, without concerns about heat-transfer distortions.

This approach may seem plausible for handling distortions due to linear processes like conduction, and we have had considerable success here; however, we have begun to make headway on characterizing convective disturbances as well. If the latter effort succeeds, we may be able to suggest one or more alternatives to refrigeration systems for dealing with convection. In summary, it is hoped that our approach will shed light on new strategies for improving the efficiency, precision and accuracy of water calorimetry and, perhaps, other dosimetric techniques where signal-to-noise challenges exist.

The following discussion begins with a consideration of heat conduction in a uniform water phantom, in which our transfer-function approach is introduced. Complications posed by natural convection are then considered. This is followed by a survey of results from our experimental and numerical studies and plans for future work.

### Theory

When a radiation beam is chopped by a shutter, the rate at which energy is deposited into a uniform water phantom at a given point in space may be written as a product of functions representing the spatial distribution of the dose rate and the time dependence imposed by the shutter. Accordingly, if convection is neglected, the resulting temperature distribution,  $T(\vec{x}, t)$ , within the phantom is obtained by solving the following heat conduction equation (see for example [3]):

$$\left(\partial_t - \kappa \nabla^2\right) T(\vec{x}, t) = \frac{\dot{D}}{c_v} g(\vec{x}) f(t), \quad (1)$$

where  $\kappa$  and  $c_v$  are, respectively, the thermal diffusivity and heat capacity (at constant volume) of water. The spatial distribution of the dose rate is represented by  $\dot{D}g(\vec{x})$ , where  $g(\vec{x})$  is bounded between 0 and 1. The function  $f(t)$  represents the action of the shutter; in our work,  $f(t)$  is usually a square wave that toggles between 0 and 1 within the interval  $0 \leq t \leq t_f$  (i.e. the duration of the experiment) and vanishes elsewhere, although for the present discussion it is arbitrary.

Since we shall be interested in the frequency response of the system, we perform a Fourier transform the time variable in Eq.1 to obtain:

$$\left(i\omega - \kappa \nabla^2\right) \tilde{T}(\vec{x}, \omega) = \frac{\dot{D}}{c_v} g(\vec{x}) \tilde{f}(\omega). \quad (2)$$

For a cubic phantom of length  $2L$  on a side, products of the form  $e^{ilkx} e^{imky} e^{inkz}$  can be used to construct solutions that satisfy insulating boundary conditions at the walls if  $l$ ,  $m$  and  $n$  are integers and  $k = \pi/L$ . By similarly decomposing  $g(\vec{x})$  as a product of Fourier series in each coordinate:

$$\begin{aligned}
g(\vec{x}) &= \sum_{l,m,n=-\infty}^{\infty} g_l(x)e^{ilkx} g_m(y)e^{imky} g_n(z)e^{inkz} \\
&= \sum_{l,m,n=-\infty}^{\infty} g_{lmn}(\vec{x}),
\end{aligned} \tag{2}$$

we obtain the following:

$$\begin{aligned}
\tilde{T}(\vec{x}, \omega) &= \frac{\dot{D}}{c_v} \left\{ \sum_{l,m,n=-\infty}^{\infty} \frac{1}{i\omega + \kappa k^2 (l^2 + m^2 + n^2)} g_{lmn}(\vec{x}) \right\} \tilde{f}(\omega) \\
&= \frac{\dot{D}}{c_v} H(\vec{x}, \omega) \tilde{f}(\omega).
\end{aligned} \tag{3}$$

The quantity in brackets in Eq. 3, abbreviated as  $H(\vec{x}, \omega)$ , is the system transfer function, and it represents the physics of heat conduction as an attenuation and phase shift for each bin in the spectrum  $\tilde{f}(\omega)$  of the shutter function.

Extending this analysis to a phantom in which convection occurs would at first seem improbable because of nonlinearities contained in the equations of motion. Even within the Boussinesq approximation, which is typically invoked in water calorimetry, nonlinear terms remain in the equations governing the time dependence of the velocity and the temperature. However, in his original study of Benard convection, Rayleigh [4] derived a set of linearized Boussinesq equations for sufficiently small temperature changes and fluid velocities characterizing incipient natural convection in thin fluid layers with fixed-temperature boundaries. Assessing conditions for neglecting higher-order terms in the perturbations (of temperature and fluid velocity) is difficult experimentally; nevertheless, we have been able to explain semi-quantitatively certain oscillatory behavior observed in our experiments using Rayleigh's analysis. And, while we have derived a transfer function appropriate for linear convection and conduction, other results presented below indicate a nonlinear convection mechanism that require consideration of higher-order terms. That work is beyond the scope of this paper; more details will be published elsewhere [5].

## Materials and Methods

The work summarized here was done using the second-generation water calorimeter under development at the National Institute of Standards and Technology (NIST). The essential details of the water calorimeter [6 and references therein], are provided here.

The water calorimeter is contained within an acrylic tank whose inner dimensions are 30 cm x 30 cm x 30 cm. The top of the tank is removable and contains an entrance window for the radiation (12 cm x 12 cm x 0.35 cm) and hardware for mounting and positioning the glass core. A magnetic stirrer that rests on the bottom of the tank can be actuated for purposes of stirring the water in the phantom in order to remove thermal gradients. The phantom is surrounded on all sides by 2 to 3 layers of 2.54 cm-thick foam insulation, all of which is contained in a shielded box made out 0.16 cm-thick sheet aluminum that is reinforced on the sides and bottom by 0.635 cm-thick plywood (the aluminum cover on

top has a 12 cm x 12 cm cutout for the beam that is covered by aluminum foil). The schematic diagram of the system is shown in Figure 3.

As noted above, the calorimeter sensors are suspended inside the phantom by brackets that are mounted to the lid. The brackets may be raised/lowered by adjusting small, threaded steel rods (roughly 0.32 cm diameter) for purposes of positioning the sensors (or, more often, a glass vessel containing the sensors) at the desired depth in the water, 5 cm in most cases. The glass vessel contains hydrogen saturated high-purity water and a small, hydrogen bubble to allow for volume changes of the water as temperature varies. The temperature probes contain negative temperature coefficient (NTC) type glass-coated bead thermistors that have a nominal diameter of 0.18 mm and a nominal resistance of 10  $\Omega$ . The thermistor beads are sealed inside thin-walled glass capillaries (inner/outer diameters = 0.3 mm/0.4 mm) that are used both to cantilever the beads into the center of the beam and to provide a conduit for electrical leads.

The thermistors are wired into opposite arms of a Wheatstone bridge circuit, in which a combination of fixed and adjustable precision resistors is used to establish balance conditions. The supply voltage for the bridge is a 1 V root-mean-squared, 100 Hz sine wave provided by a dual-phase lock-in amplifier, which also is used to detect changes in the bridge output. The sensitivity of the device is as follows: 1 Gy of dose increases water temperature by about 0.24 mK, causing a change of about 0.2  $\Omega$  in the two thermistors, resulting in about 3.5  $\mu$ V change in the voltage across the bridge.

The lock-in amplifier is controlled by a computer through an IEEE-488 interface. In most cases, the input antialiasing filter on the instrument is set for a time constant of 100 ms and a roll off of 24 dB/octave. The computer polls the lock-in for converted voltage measurements from the bridge at a sample rate ranging from 1 Hz to 5 Hz, and also controls the  $^{60}\text{Co}$  shutter via a digital input/output card wired to high-power relays. This allows us to open/close the shutter at a well-defined period and duty cycle (or a sequence of periods and duty cycles) for arbitrary lengths of time. The waveform we derive from the instrument is stored and then analyzed offline with code that calculates the magnitude and phase spectrum. The signals of interest are easily identified in the spectra as sharp spikes (Fig. 4), and their magnitudes are determined by peak-height estimation [7]. The noise floor in the immediate vicinity of each peak is used to estimate the random uncertainty in the peak height.

It remains for us to describe how to extract an estimate of absorbed dose from the Fourier transform  $\tilde{T}(\vec{x}, \omega)$  of the measured time waveform  $T(\vec{x}, t)$ . The example spectrum shown in Figure 4 consists of a series of sharp peaks at the shutter frequency and odd harmonics thereof, decaying in amplitude in a nearly  $\omega^{-2}$  fashion. A strict  $\omega^{-2}$  dependence would be expected for an integrated square wave, i.e. what we would have in the limit of negligible heat transfer. Each peak in the spectrum is the product of the desired quantity,  $\dot{D}$ , the (reciprocal of the) heat capacity of water (which is well-known) and two other functions,  $\tilde{H}(\vec{x}, \omega)$  and  $\tilde{f}(\omega)$ . The latter, being the Fourier transform of the shutter function  $f(t)$  is easily determined and can be divided out. Because the transfer function

$\tilde{H}(\vec{x}, \omega)$  contains information about the thermal response of the calorimeter components, it must be measured separately or, perhaps, obtained by means of finite-element simulations. Once it is known to sufficient precision, however, it would become possible to divide out systematic errors related to heat transfer for arbitrary timing conditions of the radiation beam. No attempt is made here to divide out the transfer function; rather, the results we present simply demonstrate its effect upon the measurements.

## Results and Discussion

We begin the survey of results with the calculated transfer functions (multiplied by  $\omega$  to get the per unit time response) shown in Figure 2, which highlight the distortions attributable to heat conduction and employ plotting conventions used in later figures that require some explanation. Transfer functions, being a measure of frequency response, usually are plotted versus frequency; however, because we typically work with the shutter period, we have opted for a time axis in Figure 2. The time, in that case, refers to the exposure time per period of the shutter (e.g.  $\omega = 2\pi/T = 0.05236$  rad/s corresponds to a period of  $T = 120$  s or an exposure time  $T/2 = 60$  s). Several similar transfer functions appear in the plot, and all show large deviations of the apparent dose rate from the nominal value at larger exposure times, as should be expected. For metrological applications, exposure times rarely exceed 120 seconds because one expects undesired heat-transfer effects to increase with prolonged irradiation. Our calculations indicate much smaller systematic effects at those lower exposure-time scales – below 1 % in most cases – but show them to be part of a much larger, and perhaps surprisingly, oscillatory trend with exposure time of the system transfer function (in which all spatial modes have been summed).

The numerical calculations were performed using finite-element methods to simulate a thin-walled cylindrical vessel containing distilled water and surrounded by stirred water represented by a variable thermal conductivity coefficient. The finite-element output duplicated exactly the result of one-dimensional analytical calculations of a localized, square wave heat source in a uniform phantom. Since this study was intended to be a more qualitative investigation of the effects of heat transfer in water calorimeters, certain simplifications of the problem were adopted. For example, the radiation heating was simulated with a coaxial, uniform heat source term. Also, the variable conductivity referred to above was intended to mimic the effect of stirring the phantom would have on conduction of heat away from the water inside the glass core without the attendant complications of a full simulation of forced convection. As might be deduced from the plots in Figure 2, this has proved to be a useful adjustable parameter in comparisons between simulated and experimental data because it allows us to vary the scale of the transfer function. It also has some physical motivation from the simple fact that increasing the effective thermal conductivity of the external water (i.e. the water outside the vessel) accelerates the redistribution of heat in the phantom in a manner that would be identical to perfect stirring.

Such a comparison of simulated transfer functions with measurements of apparent dose rate (normalized to the nominal value obtained from ion-chamber measurements) is shown in Figure 5. The measurements were taken using two (cylindrical) glass vessels

with different radii over a wide range of shutter periods. For each vessel, the variation of the apparent dose rate with shutter period is quite similar to the corresponding finite-element output. For both radii, the external thermal diffusivity in the calculation is the same (of order 10 W/m-K); only the radii are adjusted within the simulation, and the output is found to track the corresponding changes in the experimental data. The simulations were not as successful at predicting the amplitude of oscillations observed in the apparent dose rate. We are looking into possible causes for this disagreement (e.g. calculations with a realistic, three-dimensional model of the beam).

According to the results summarized in Figures 2 and 5, the frequency response of the calorimeter is reasonably well explained by the physics of conduction, and, until recently, we believed that this might be sufficient for characterizing all observed systematic errors. Subsequent investigation of spectra at extended exposure times, however, revealed some anomalies that we believe are attributable to convection. The spectrum plotted in Figure 6 shows such an anomaly in the case of a very long shutter period (70 minutes): the appearance of even harmonics. With linear processes such as conduction, the output spectrum must be proportional to the input spectrum; accordingly, if the input spectrum consists of a fundamental frequency and its odd harmonics, then the appearance of even harmonics in the output is evidence of a nonlinear mechanism. These anomalous, even-harmonic peaks were observed in spectra for exposure-times above 1500 s, and were found to grow with increasing exposure time. Thus, we decided to conduct a series of measurements without the glass vessel present to see whether the nonlinearity would intensify, as might be expected if the mechanism were related to convection. Figure 7 shows the resulting spectrum obtained at an exposure time of 3600 s, which indicates considerable enhancement of the effect over that observed with the glass vessel in place. In fact, as shown in Figure 8, without the glass vessel present, anomalous peaks are clearly discernible at a much shorter exposure time of 240 s.

At the present time, we believe that these anomalous peaks are explained theoretically by the influence of the convection term,  $\bar{u} \cdot \nabla T$ , in the modified equation of heat conduction associated with the Boussinesq approximation (here,  $\bar{u}$  represents fluid velocity). Qualitatively, for very weak convection, the time dependence of  $\bar{u}$  would be expected to mirror that of the temperature gradient,  $\nabla T$ , which would be primarily determined by the shutter function,  $f(t)$ . Thus, if the shutter function consists of only odd harmonics, the convection term, being a product of similar factors, would yield even harmonics. As noted above, a more thoroughgoing treatment of this problem is to be published elsewhere; however, we cite here other experimental evidence that appears to be amenable to Rayleigh's linear theory of convection. Also noted above, Rayleigh's theory provides an estimate of the frequency of small oscillations (of temperature and velocity) of a convection/conduction system in equilibrium that is subject to small disturbances. Experimentally, with bare thermistors in open water (without the glass vessel), we obtained the time waveform shown in Figure 9, in which slowly decaying oscillations are observed. The observed decay time and oscillation period are estimated as 670 s and 600 s, respectively. If we assume that the disturbances are caused by the temperature gradient of 0.75 mK over the top 1 cm in the depth dose curve build up region, we can reproduce the experimental decay constant and oscillation period from Rayleigh's analysis

employing a single spatial mode. This suggests that contributions from higher-order spatial modes are small.

Similar estimates of mean oscillation frequency and decay time can be obtained from the frequency-domain manifestation of these oscillations: i.e. the approximately Lorentzian profile defining the envelope of the peaks in Figure 7. Therefore, either time- or frequency-domain data indicate that the convective movement is very similar to that of a damped, simple harmonic oscillator. Additional effort with finite-element models should help us to resolve more precisely how convection is occurring within the phantom and within the glass vessel. If the resulting physics can be related to simple electrical and/or mechanical models, we may be able to generate a digital filter for mathematically removing the effect.

In conclusion, the frequency-domain approach outlined here for analyzing data from water calorimeters shows considerable promise for identifying and differentiating systematic errors due to heat conduction and convection, and may prove to be useful in designing algorithms that may work in place of or alongside existing experimental remedies for removing such effects.

## References

- [1] J. P. Seuntjens and A. R. DuSautoy, Review of calorimeter based absorbed dose to water standards, Standards and Codes of Practice in Medical Radiation Dosimetry (Proc. Int. Symp. Vienna, 2002), IAEA Vienna (2003) IAEA-CN-96-3.
- [2] A. Krauss, The PTB water calorimeter for the absolute determination of absorbed dose to water in  $^{60}\text{Co}$  radiation, *Metrologia* **43** 259-272 (2006).
- [3] H. S. Carslaw and J. C. Jaeger, *Conduction of heat in solids*, Oxford Press, London (1978).
- [4] J. W. (Strutt) Rayleigh, On convection currents in a horizontal layer of fluid, *Phil. Mag.*, **XXXII** 529-546 (1916).
- [5] R. E. Tosh and H. H. Chen-Mayer, A Transfer-function Approach to Characterizing Heat Transport in Water Calorimeters Used in Radiation Dosimetry, Proc. ITCC29/ITES17 Conference, Birmingham, AL, June 2007, in preparation.
- [6] H. H. Chen-Mayer, K. W. O'Connor, R. Minniti, R., and K. P. Gall, Evaluation of a Second Generation Dosem-Type Water Calorimeter for Absorbed Dose in a  $^{60}\text{Co}$  Beam at NIST, Proceedings of the Workshop on Recent Advances in Absorbed Dose Standards, ARPANSA, Melbourne, Australia, 19-21 August 2003 (<http://www.arpansa.gov.au/pubs/absdos/chen.pdf>).
- [7] C. Lanczos: *Applied Analysis*, Dover, pp. 186-187, (1988).

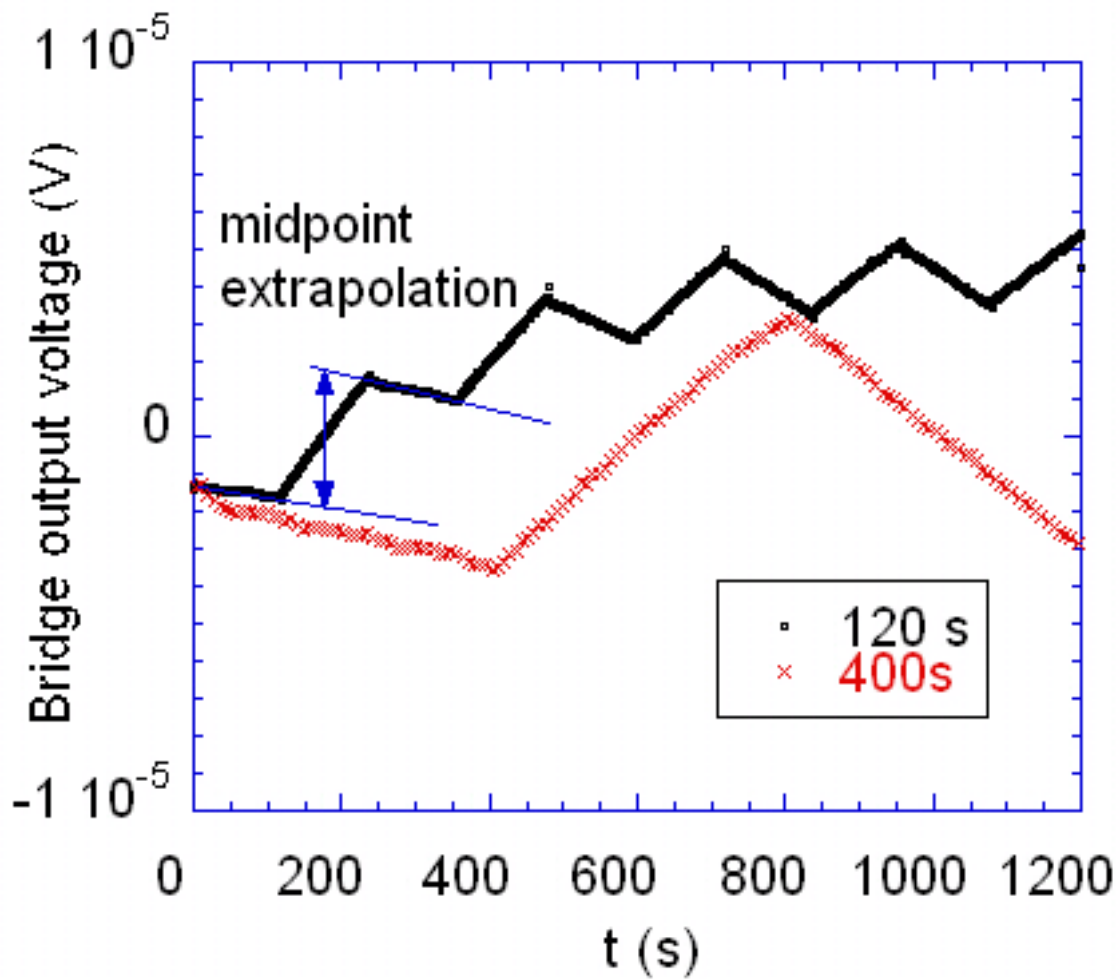


Fig. 1. Time domain waveform showing responses for 120 s and 400 s irradiation times. The midpoint extrapolation method is illustrated in the 120 s waveform, where a pre and post drift regions are fitted to straight lines, and the difference at mid radiation point is evaluated to represent the temperature rise caused by the radiation.

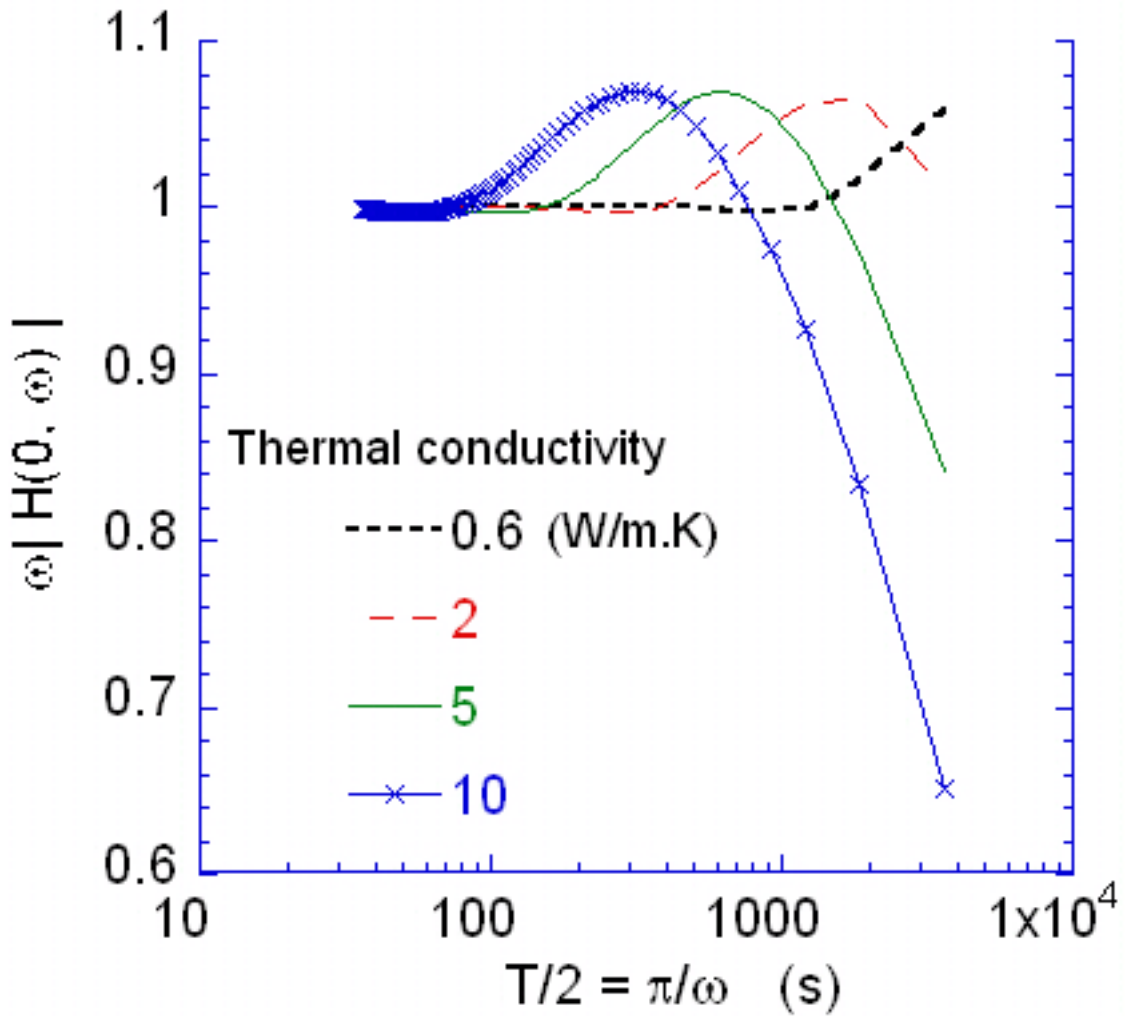


Fig. 2. Analytically calculated transfer functions (multiplied by  $\omega$ ) at various rate of heat conduction in one dimension. The horizontal axis is plotted as the half period,  $T/2$ , where  $T$  is related to angular frequency by  $T = 2\pi/\omega$ . The thermal conductivity (in W/m.K) is artificially varied from 0.6, the true value, to higher values to simulate stirred water which carries the heat away more rapidly. The peak of the transfer function is shifted accordingly, occurring at a lower  $T/2$  as the thermal conductivity increases.

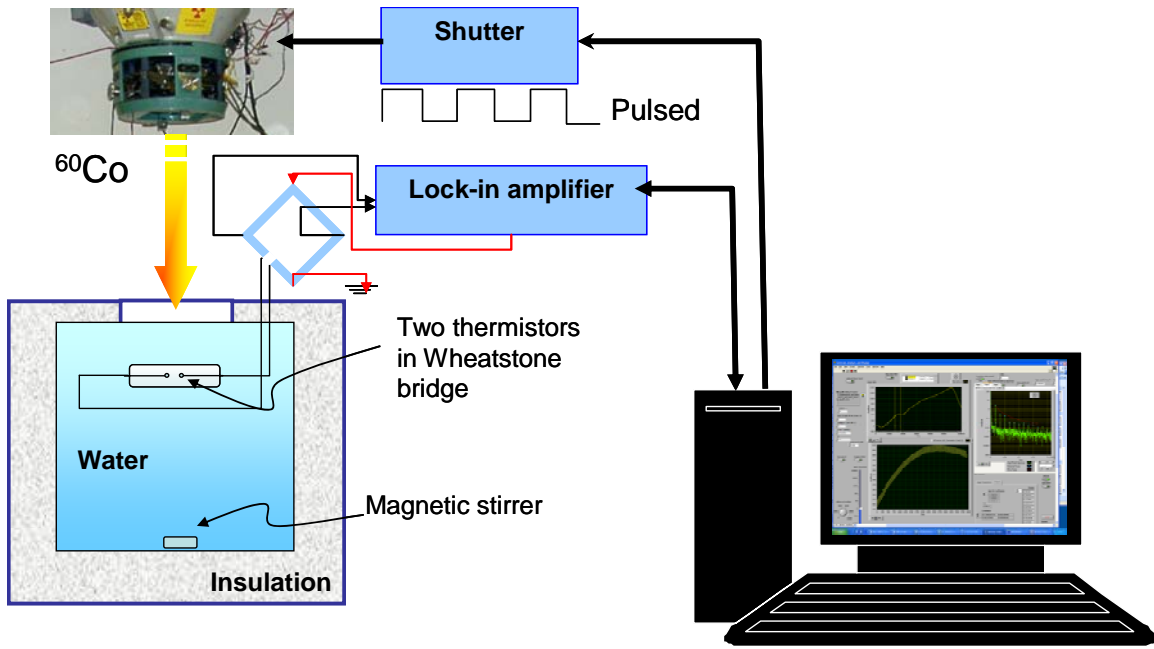


Fig. 3. Schematic drawing of the experimental system.

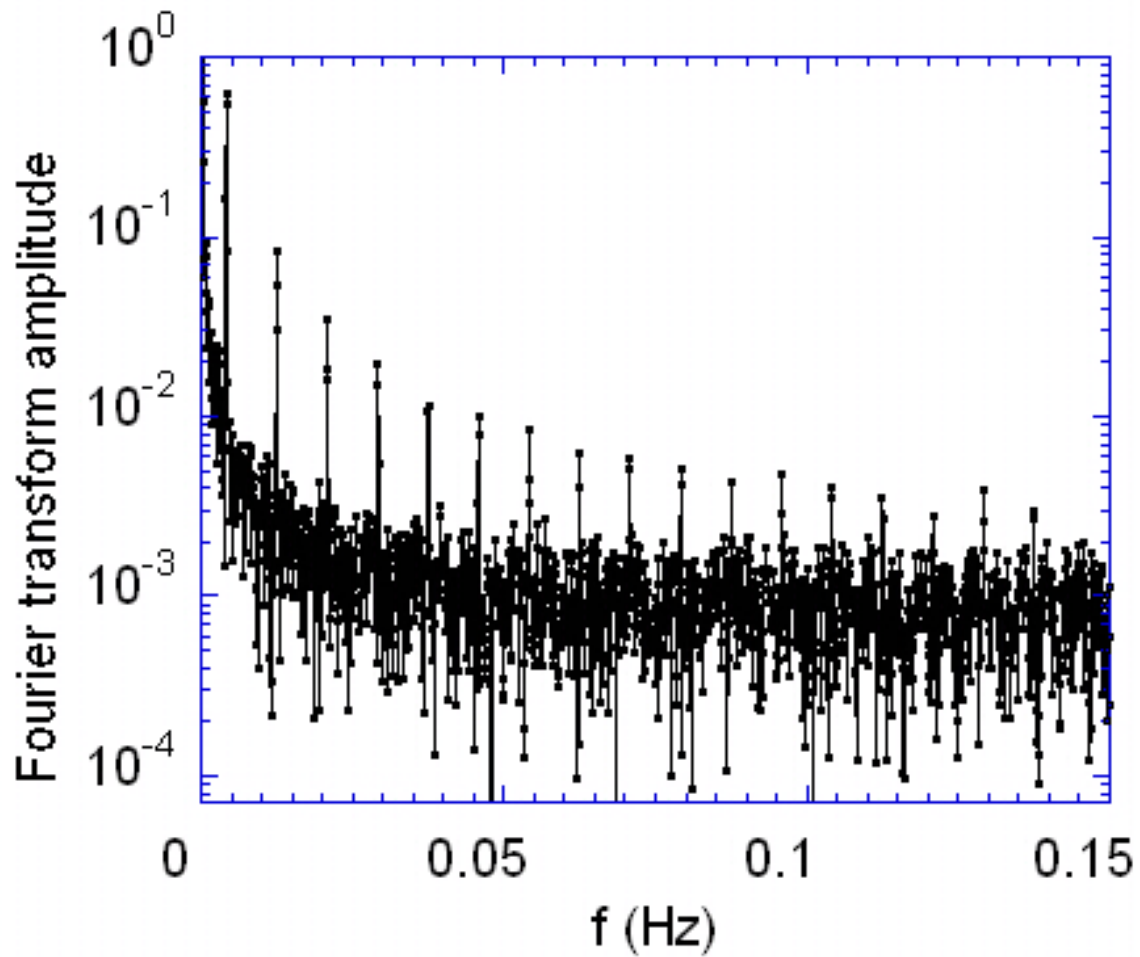


Fig. 4. Fourier transform magnitude spectrum ( $f = \omega/(2\pi)$ ) of the 120 s on/off time waveform from Fig. 1. The fundamental frequency is at  $f_0 = 1/(240 \text{ s}) = 0.004166$  Hz. Only the odd harmonics of  $f_0$  are present, characteristic of a linear response to a square wave excitation.

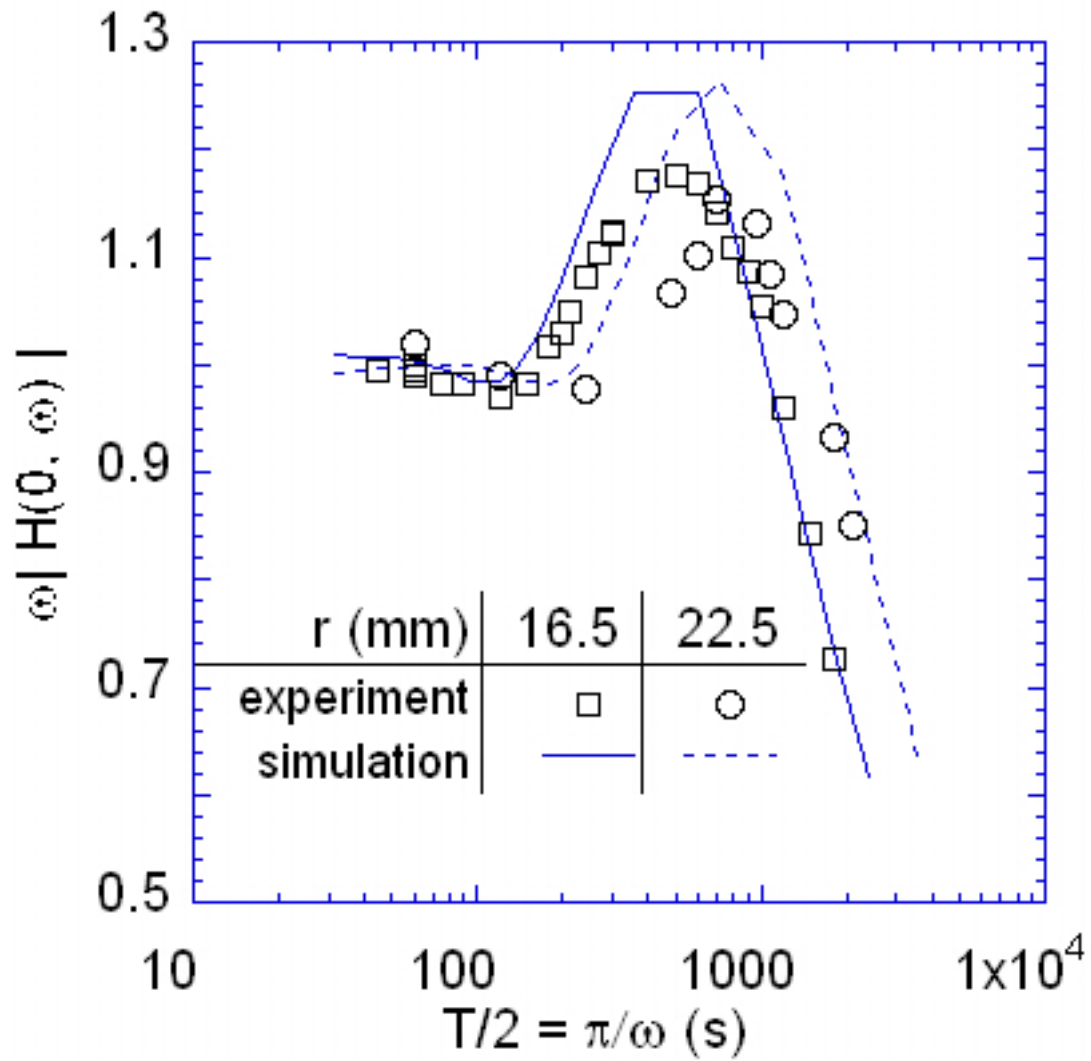


Fig. 5. Transfer functions (multiplied by  $\omega$ ) obtained experimentally and numerically with two vessels. Again the horizontal axis is the half shutter period  $T/2$  ( $T = 2\pi/\omega$ ) for convenience of comparison with experimental conditions.

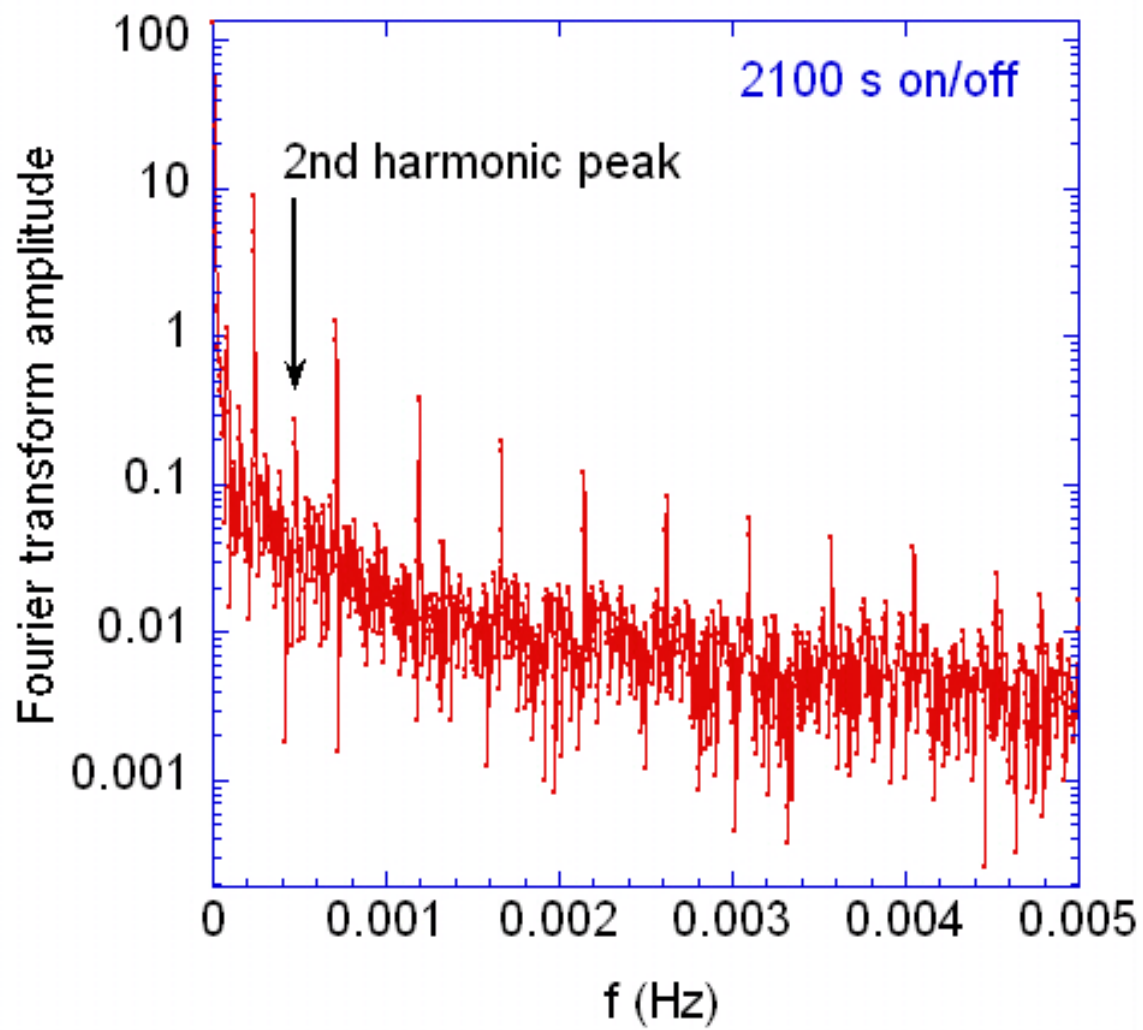


Fig. 6. Even harmonics observed at long radiation times (2100 s) within a glass vessel (45 mm diameter).

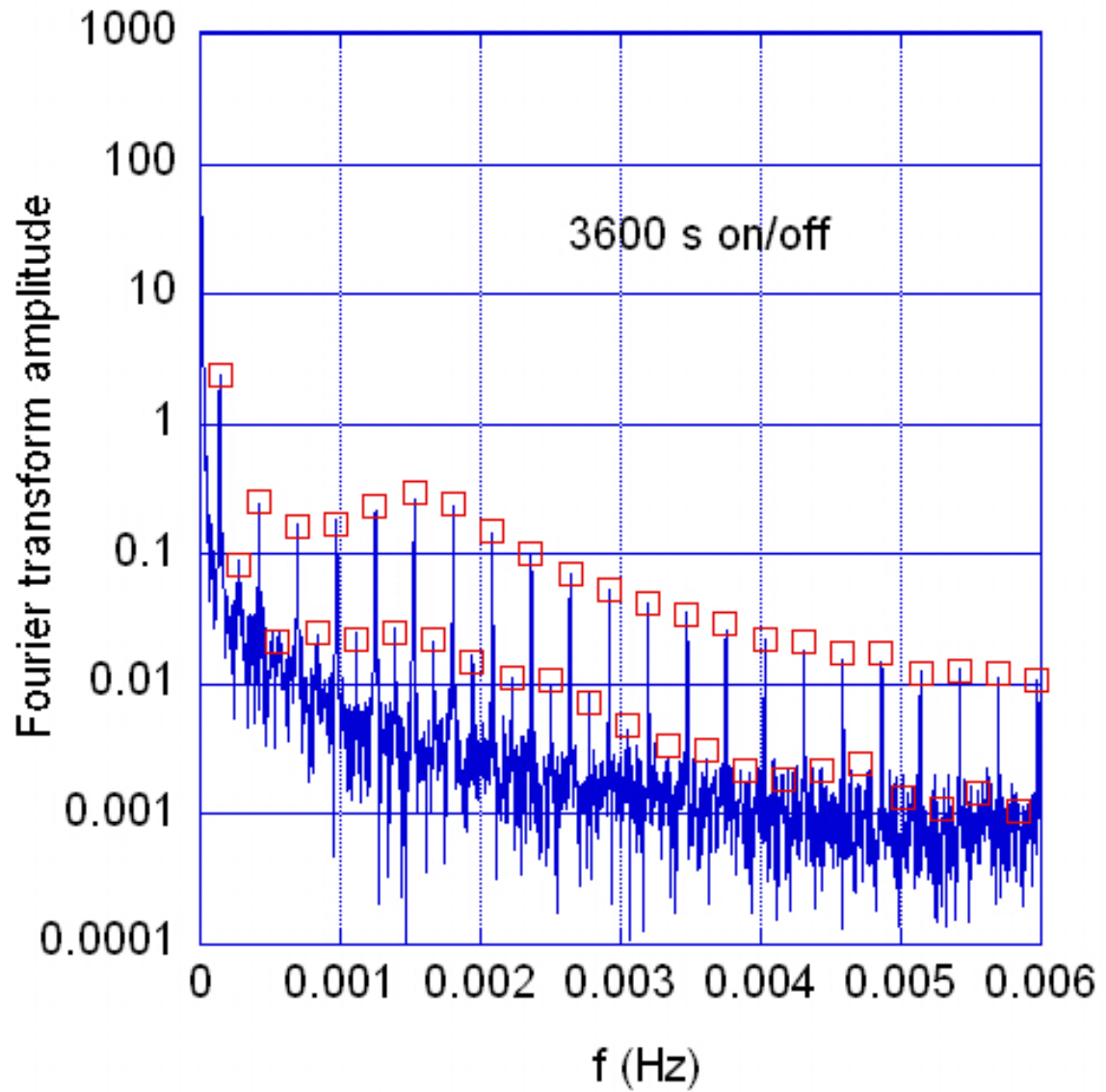


Fig. 7. Fourier transform magnitude spectrum of a waveform at long radiation times (3600 s) measured by a thermistor in open water showing structures in the envelope function.

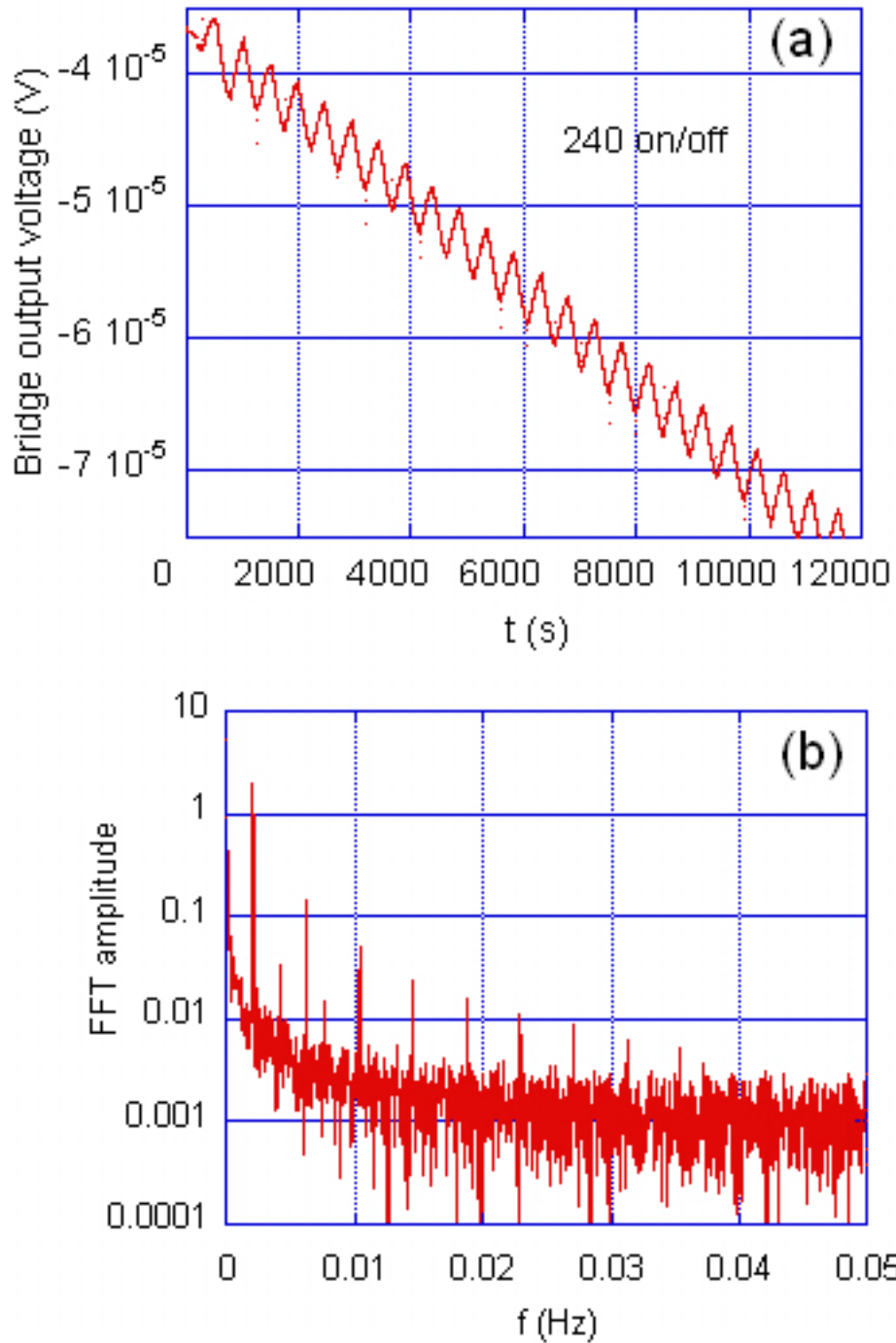


Fig. 8. In open water, signs of convection observed at a radiation time as low as 240s. (a) Time domain waveform. (b) Frequency spectrum showing even harmonics.

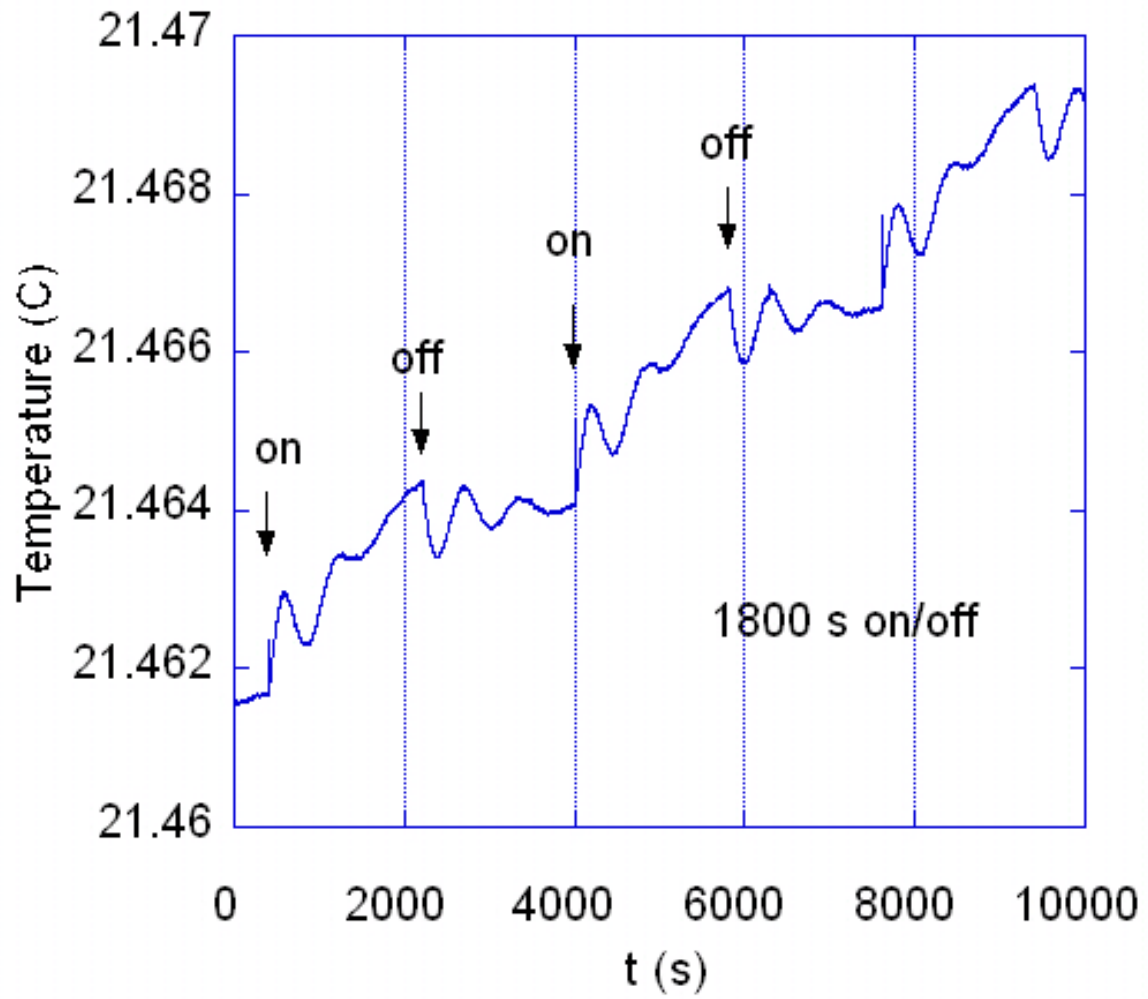


Fig. 9. Convection ringing observed in open water at 1800 s on/off radiation cycles.